Revised Manuscript ID APCATB-D-19-03259

New insights into the role of Pd-Ce interface for methane activation on monolithic supported Pd catalysts: A step forward the development of novel PGM Three-Way Catalysts for natural gas fueled engines

Jianjun Chen,[a] Yang Wu,[a] Wei Hu,[e] Pengfei Qu,[b] Guochen Zhang,[b] Pascal Granger,[c *] Lin Zhong [b *], and Yaoqiang Chen [a, b, d *]

[a] Institute of New Energy and Low-carbon Technology, Sichuan University, Chengdu 610064, China
[b] College of Chemical Engineering, Sichuan University, Chengdu 610064, China
[c] Univ. Lille, CNRS, Centrale Lille, ENSCL, Univ. Artois, UMR 8181 - UCCS - Unité de Catalyse et Chimie du Solide, F-59000 Lille, France
[d] College of Chemistry, Sichuan University, Chengdu 610064, China
[e] Institute of Atmospheric Environment, Chongqing Academy of Environmental Science, Chongqing 401147, China

* Corresponding authors: Pascal Granger (Email: pascal.granger@univ-lille.fr; Fax: +33-320436561), Lin Zhong (Email: zhonglin@scu.edu.cn; Fax: +86-28-85418451), Yaoqiang Chen (Email: nic7501@scu.edu.cn; Fax: +86-28-85418451)

Abstract:

This study reports a significant impact of the calcination temperature on the performances of Pd/Al_2O_3-CeO_2 Three-Way-Catalysts to treat exhaust from natural gas fueled vehicles. Calcination from 550 °C to 950 °C led to Pd particles in the range 1.9-8.5 nm. It was found that PdO can be reduced to more active Pd^0 species under stoichiometric NGV conditions. More specifically, the 1.9 nm Pd particles, developing stronger Pd-Ce interaction were found more reducible and correspond to enhanced catalytic properties towards methane abatement. At high calcination temperature, corresponding to larger Pd particles, the deterioration of the Pd-Ce interface is accompanied with lower TOF jointly with higher activation barriers. Accordingly, the Pd^0-PdO interaction becomes prevalent to activate methane. Based on these observations, it was concluded that Pd^0-Ce and Pd^0-PdO interface related to the Pd particle size may be considered as criteria for identifying the performance of Pd-based NGV catalysts.

Keywords: CH_4 activation; Pd-Ce interface; Pd-PdO interaction; Pd^0 active phase; NGV Three-Way Catalyst.

1. Introduction

Nowadays, natural gas fueled vehicles (NGVs) are an important alternative to gasoline and diesel fueled vehicles. The advantages of NGVs are lower greenhouse gas emissions [1, 2], lower NO_x emissions [3] and nearly no particle matter formation. However, the unburned CH_4 from NGV exhausts has about 21 times more effect on global warming than an equivalent mass of CO_2 [4]. Therefore, this CH_4 pollutant must be efficiently eliminated through appropriate catalytic end-of-pipe technology to meet the increasingly stringent emission regulations (China 6, Euro 6, and US Phase 2 Heavy-Duty Greenhouse Gas for 2021-2027) [5]. The development of highly efficient methane emissions-control catalysts still remains remarkably challenging because of the high chemical stability of methane [6-8]. It is currently observed that supported Pd-based catalysts are highly effective at reducing concentrations of CH_4 in exhaust streams and has attracted a continuous attention in the past few decades [9, 10].

Generally, many factors affect the activity of CH_4 conversion of Pd-based catalysts, such as their physicochemical properties, the preparation method, catalyst history, reduction properties, and the extent of metal-support interaction [11-14]. One of the most important factors governing the efficiency of Pd-based catalysts is the particle size, which was closely associated with the Pd chemical state and the accessibility of Pd active species [15, 16]. The effect of Pd particle size on the CH_4 removal activity has attracted considerable attention. Hicks et al. [17] investigated CH_4 oxidation under lean conditions over Pd/Al_2O_3 with a wide range of Pd particle size. They found that the Turn-Over-Frequency (TOF) and activation energy over small Pd particles (~1.4 nm) was 0.02 s^{-1} and 27 kcal/mol, respectively. On the other hand, the TOF

increased to 1.3 s^{-1} over larger Pd particles (~4.0 nm) whereas the activation energy remained unchanged, i.e. 29 kcal/mol. These results clearly demonstrated that the catalytic activity for CH_4 oxidation over Pd/Al_2O_3 is particle size dependent. Such structure sensitivity was also confirmed on a wider range of Pd particle size from 1.5 to 20 nm [18]. In agreement with these observations, Iglesia et al. [19] concluded that the strong Pd-O bond in small PdO_x crystallites can be responsible for the decreased CH_4 combustion activity with decreasing PdO_x crystallite size under lean conditions because the reaction would obey a Mars-Van Krevelen redox mechanism involving methane activation on the surface of PdO_x crystallites. However, some controversies on the nature of active sites and the structure sensitivity of this reaction still arise. Indeed, Ribeiro et al. [20] reported that the methane oxidation reaction was insensitive to the structure of the catalyst by studying large single-crystal Pd model catalysts. Furthermore, these authors also confirmed the structure insensitivity of CH_4 oxidation reaction by measuring the activity of methane conversion under lean conditions over Pd supported on Al_2O_3 and ZrO_2 [21]. The different observations of the effect of Pd particle size on CH_4 oxidation activity can be complicated due to the differences in the energy of Pd-O bond at varying PdO crystallite size.

Although plenty of published papers have been devoted to the impact of Pd size on the activity over Pd catalysts, this issue is still controversial. It should be noted that the differences in the experimental conditions may result in different observations. Up to now, methane oxidation over Pd catalysts has been essentially investigated in large excess of oxygen and the Pd particle size found as a critical factor. In three-way conditions, the air-to-fuel ratio near the stoichiometry is always fluctuating during sudden acceleration and deceleration, inducing changes in O_2 concentration in the exhaust gas, thereby making the reaction of CH_4 conversion more complex [1, 2, 6,

22]. In such operating conditions previous investigations are more scarce and the particle size dependency on the rate has not been clearly established likely due to complexity of the surface and subsequent equilibration under typical TWC conditions. The interactions of Pd with other components such as cerium in alumina support could play a key role in the activity of CH_4 conversion. Interestingly, our recent work [8, 23] found that the metallic Pd species was much more active than PdO for the abatement of CH_4 over supported Pd catalysts on Ce-modified Al_2O_3 in stoichiometric conditions. In this work, we have attempted to examine the particle size effect of Pd nanoparticles on the catalytic activity of CH_4 abatement under stoichiometric NGV conditions. The relationship between Pd particle size and catalytic properties was investigated by XRD, STEM, HRTEM, TPO, CH_4-TPR, XPS, and *in situ* DRIFTS starting from catalysts calcined at various temperatures. It has been be found that small PdO crystallites was more prone to produce large amount of Pd^0 active sites during reaction process, resulting in better catalytic activity of CH_4 elimination. However, it has been found that probably more complex kinetic features can be governed by the specific interactions of those metallic particles with ceria and/or with PdO which supply oxygen species having various reactivities towards methane activation.

2. Experimental

2.1. Catalyst Preparation

A commercial γ-Al_2O_3 (139 m^2/g) was calcined in air at 900 °C for 8 h. 3 wt.% CeO_2 modified alumina was prepared (5 grams) by incipient wetness impregnation using

$Ce(NH_4)_2(NO_3)_6$ (Sigma Aldrich) as cerium precursor salt dissolved in water. The corresponding volume and the concentration of Ce^{4+} in the solution for the impregnation was 5.0 mL and 0.174 M, respectively. The solid thus obtained after filtration was dried at 110°C and calcined in air at 550 °C for 3 h. The as-prepared materials was used as support then impregnated with a 15.6 wt.% of $Pd(NO_3)_2$ solution (Heraeus) to obtain supported Pd catalysts containing 1 wt.% Pd. The corresponding volume and Pd^{2+} concentration of the solution for this impregnation was 5.0 mL and 0.094 M, respectively. The solvent was removed by a rotary evaporator at 60 °C for 12 h. The solid precursor was further dried in air at 110 °C for 12 h then calcined in air at 550 °C, 800 °C, 850 °C, 900 °C, and 950 °C for 5 h (heating rate of 4 °C/min) respectively. The calcined samples were labeled Pd/Al-Ce(x) with x representing the calcination temperature. The monolithic catalysts were prepared according to our previous work [24]. Typically, the monolith substrate (Corning, 400 cells /in^2, volume 2.0 mL, length 25 mm, diameter round 11 mm and the wall thickness 0.10 mm) was vertically immersed into the wash-coat slurry (~0.30 g catalyst powder/mL) for 1-1.5 min. Afterwards, the excess slurry was removed using a compress air feed. After drying at 120 °C for 1 h, the procedure was repeated till to obtain the desired Pd loading of ~ 1.7 g/L (50 g/ft^3). The monolithic catalysts were then dried and calcined at 550 °C for 3 h in air.

2.2. Physicochemical Characterization

Nitrogen physisorption (Quantachrome, Autosorb SI) experiments was carried out at -196°C to estimate the Brunauer-Emmett-Teller (BET) surface area and the total pore volume according to the BET model and Barrett-Joyner-Halenda (BJH) method

respectively. Powder X-ray diffraction (XRD) patterns were recorded on a Rigaku DX-2500 diffractometer (Japan Science, Rigaku, Tokyo, Japan) using Cu Kα radiation (λ = 0.15406 nm) in the region of 2θ =10-80° at 40 kV and 40 mA of X-ray tube.

CO chemisorption measurements were performed according to a pulse technique to determine the Pd dispersion (D_{Pd}). Sample (200 mg) was initially preheated in 5 vol.% H_2 in He at 450°C for 1 h and then degassed in He for 0.5 h. Measurements were performed at -78.5°C under He in ice/ethanol refrigerant to prevent CO adsorption on the support [25, 26]. Then, CO pulses (11.10 μmol/pulse) were injected into the catalyst sample in a flow of He while monitoring the effluent with a thermal conductivity detector (TCD). The Pd dispersion was calculated from the total CO uptake by assuming a stoichiometric ratio CO/Pd = 1 [27].

Pd particle size was measured by using a Tecnai G^2 F20 S-TWIN Transmission electron microscope (TEM) (FEI Company, USA, 200 kV accelerating voltage). The samples were prepared by spreading a drop of methanol suspension of Pd catalysts and further dried in air.

Temperature programmed oxidation (TPO) experiments were conducted in a quartz microreactor. Prior to experiments, the catalyst sample in powder form (~100 mg) was treated in flowing He (30 mL min^{-1}) at 500 °C for 0.5 h and cooled down to 300 °C. TPO experiments were conducted under a flow of 2 vol.% O_2/He (30 mL min^{-1}). The sample was heated to 950 °C at 10 °C min^{-1} then cooled down with the same rate velocity. The oxygen uptake/release was monitored with a TCD.

Methane Temperature Programmed Reduction (CH_4-TPR) was carried out in a quartz flow micro-reactor equipped with a Fourier Transform Infrared (FTIR) analyzer. Prior to CH_4-TPR experiments, each sample (50 mg) was preliminary heated at 450 °C for 30 min in He with a flow of 50 mL min^{-1}. After cooling down to 150 °C in flowing He,

the CH_4-TPR experiment was conducted from 150 to 400 °C in a flow of 1 vol.% CH_4/He (50 mL min^{-1}) with a temperature gradient of 10 °C min^{-1}.

X-ray photoelectron spectroscopy (XPS) measurements were performed on a Kratos XSAM 800 spectrometer equipped with Mg Kα radiation (1253.6 eV) operated at 13 kV and 20 mA. The C 1s core level at 284.6 eV was used to calibrate B.E. values. The preparation protocol for XPS analysis on preactivated samples is displayed in Fig. S1 in Supplementary Material. Typically, the feed gas was cut off immediately once the pre-reacted procedure finished. In order to preserve the catalyst state, the samples were quickly immersed in liquid nitrogen to quench the catalyst with no longer exposure to air [14, 28]. The obtained catalysts were introduced into the XPS vacuum chamber for analysis.

In situ diffuse reflectance infrared Fourier transform spectroscopy (DRIFTS) of CO adsorption was collected on a Nicolet 6700 IR spectrometer equipped with a KBr window and a gas-dosing system to perform measurements in controlled gas environments at atmospheric pressure. The spectra were recorded with a resolution of 4 cm^{-1} and 64 scans in Kubelka-Munk units. A similar pretreatment of the catalyst as that displayed for pulse CO chemisorption measurements was implemented. After cooling down to 30 °C in a flow of He (30 mL min^{-1}), the sample was subsequently exposed to 1 vol.% CO/He (30 mL min^{-1}) at 30 °C for 10 min till saturation coverage. The IR cell was finally purged under a flow of helium before recording IR spectra.

2.3. Catalytic measurements

The catalytic properties of monolithic catalyst samples were evaluated in a multiple

fixed bed continuous flow reactor operated at atmospheric pressure. The inlet gas temperature of the catalyst was measured by a K-type thermocouple. The gases were fed using a series of mass flow controllers. The total inlet flow rate was 1.68 L min^{-1}, corresponding to a gas hourly space velocity (GHSV) of 50,400 h^{-1}. The feed gas composition close to real exhaust composition at the stoichiometry ($\lambda = 1$) was 1000 ppm CH_4, 5000 ppm CO, 930 ppm NO, 4035 ppm O_2, 10 vol.% H_2O, 10 vol.% CO_2 balanced with N_2.

The experimental protocol included different steps starting from a pre-activation thermal treatment under reaction mixture at 500 °C for 5 h. Subsequently, the monolithic catalyst samples were quickly cooled through immersion in liquid nitrogen to quench the catalyst with no longer exposure to air for preserving the catalysts state [14]. The catalysts were tested in the reaction gas and the outlet gas mixture was online analyzed with a FTIR analyzer (Thermo Fisher Scientific, Antaris IGS-6700), calibrated at 940 Torr and 165°C. The calibration pressure was maintained by a pressure controller at the outlet of the FTIR. The calculation of conversion (X_i) used the concentration of the reactant i monitored by the FTIR analyzer according to Eq. (1).

$$X_i = (C_{i,\,inlet} - C_{i,\,outlet}) / C_{i,\,inlet} \quad (1)$$

where $C_{i,\,inlet}$ and $C_{i,\,outlet}$ were the volumetric concentration of i species in the inlet and outlet gas mixture respectively. The reproducibility and sustainability was verified on Pd/Al-Ce(550) from multiple scans in transient and steady state conditions as illustrated in Figs. S3 and S4 reported in Supplementary Material.

3. Results and Discussion

3.1. Bulk and structural properties vs. surface functionalities for methane activation

3.1.1. Structural properties

XRD patterns recorded on calcined Pd/Al-Ce(x) are presented in Fig. 1. Broad XRD lines appear associated to the characteristic reflections of γ-alumina (JCPDS 29-1486). They likely overlap those corresponding to the cubic structure of CeO_2 at 2θ values of 28.5°, 33.0°, 47.4° and 56.2°. Anyway, the (111) reflection at 2θ = 28.5° ascribed to CeO_2 (JCPDS 34-0394) appears distinctly. The crystallite size of CeO_2 has been calculated from the Debye-Scherrer equation by using this (111) reflection and the estimates reported in Table 1 were found to vary in the range 5.3-9.2 nm. Additional reflections appear at increasing calcination temperature at 2θ values near 34.0 and 54.9° ascribed to bulk PdO species (JCPDS 43-1024). It is worthwhile to note that these reflections are no longer observed on Pd/Al-Ce(550) and Pd/Al-Ce(800) likely due the formation of smaller undetectable PdO clusters. Indeed, small crystallites, below 2–3 nm, cannot be easily detected from XRD analysis [29]. The intensification of the (101) reflection typical of PdO at 2θ = 34.0° (see Fig. 1b) underlines a significant crystallite growth jointly with a weakening of their thermal stability. As a consequence, weak (111) reflection at 2θ = 40.1° appears corresponding to bulk Pd^0 species (JCPDS 46-1043) reflecting a partial decomposition of PdO to Pd^0 when the calcination is performed above 850°C.

The PdO crystallite sizes was estimated by using the Scherrer equation from the most intense (101) reflection leading to values varying in the range 7.3-10.9 nm. In order to get more insights into the segregation of small metallic/oxidic nano-sized Pd

particles STEM analysis was performed. The STEM images for the catalysts were shown in the Fig. 2. Pd size distribution was established by counting more than 200 isolated particles for each catalyst. A spherical shape was also assumed. As summarized in Table 1, the Pd particle size varies in the range 1.9-8.5 nm when the calcination temperature shifts from 550°C to 950°C in rather good agreement with the evolution observed from XRD analysis.

3.1.2. Particle size dependency of thermal stability of supported nano-sized PdO_x clusters: Importance of the Pd-Ce interaction

Thermal stability of PdO_x clusters was investigated from TPO measurements. Fig. 3 illustrates the reversible PdO ⇆ Pd^0 transformation. At a first glance, the oxygen release during the heating process can be ascribed to thermal PdO decomposition (Fig. 3a) [30]. Two apparent maxima appear distinctly on Pd/Al-Ce(900) and Pd/Al-Ce(950) corresponding to the decomposition PdO crystallites of respectively 9 and 10.9 nm with a slight shift to higher temperature on this latter sample which seems in rather good agreement with a two-step decomposition process as reported elsewhere on Pd/Al_2O_3 [30]. As seen, a two steps re-oxidation process also occurs on all catalysts (Fig. 3b). Let us note that this re-oxidation takes place at lower temperature on samples calcined at low temperature, i.e. typically on Pd/Al-Ce(550). More complex observations appear for small PdO particles due to the observation of an extra oxygen production at higher temperature and a delay on PdO decomposition. Indeed, it can be clearly seen from Fig. 3a that smaller PdO crystallites on Pd/Al-Ce(550) are more resistant to thermal decomposition into Pd^0. The quantification and comparison of oxygen uptake and release during the heating and cooling steps respectively is useful especially to identify hypothetical extra sources of oxygen

production. Data reported in Table 2 reveal that the normalized O_2 release values on Pd/Al-Ce(550) and Pd/Al-Ce(800) of respectively 59.8 and 54.7 μmol/g_{cat}, are slightly higher than the theoretical value for a complete decomposition of PdO to Pd^0 (47.0 μmol/g_{cat}). On the other hand, underestimated values are observable on larger PdO crystallites, i.e. Pd/Al-Ce(850), Pd/Al-Ce(900) and Pd/Al-Ce(950). The extra oxygen release on samples calcined at low temperature suggests desorption of labile oxygen species from ceria. Accordingly, this comparison could reflect a weakening of the Ce-O bond thanks to a stronger Pd-support interaction leading to enhanced oxygen mobility [31, 32]. The comparison of oxygen released and captured during heating and cooling steps do not converge to the same value which is expected owing to additional O_2 production at least on ceria for small Pd particles. Although one cannot rule out this support effect on catalyst samples characterized by larger particles, the lower O_2 uptake and release could be more related to incomplete re-oxidation of large metallic Pd particles [33]. This latter explanation seems consistent with the detection of weak (111) reflection ascribed to bulk metallic Pd species from XRD analysis especially one calcined samples above 850°C.

HRTEM images were recorded on Pd/Al-Ce(550) and Pd/Al-Ce(950) (Fig. 4). On all images, the cubic structure of CeO_2 was identified from the lattices fringes of the (111) crystal plane characteristic of this structure (0.31 nm). Palladium oxide particles were also identified through the measurement of lattice fringes associated with the (100) and (101) crystal planes corresponding to 0.30 nm and 0.26 nm respectively. As seen, a larger interfacial perimeter between Pd nano-sized particles and ceria can be defined for Pd/Al-Ce(550) in comparison with Pd/Al-Ce(950). Although this observation has not been statistically verified, it seems consistent with quantitative analysis of TPO experiments showing an extra-production of oxygen on Pd/Al-

Ce(550). From this comparison one can hypothesize that enhanced oxygen mobility could be related to a larger interfacial perimeter.

3.1.3. CH_4-Temperature-Programmed Reduction experiments (CH_4-TPR).

Generally, catalysts with excellent reduction properties are beneficial for the conversion of CH_4 from NGVs exhaust emissions [8]. The formation Pd^0 during CH_4 conversion reaction was closely related to the reducibility of nano-sized PdO clusters being size dependent. As reported elsewhere by Lin et al. [32], small PdO particle sizes in strong interaction with Ce-based supports can present outstanding redox properties and favor the reduction of PdO to Pd^0. In order to clarify the reducibility of different PdO crystallite sizes on calcined Pd/Al-Ce(x) catalysts in the course of the pre-activation thermal treatment, methane-temperature-programmed reduction (CH_4-TPR) measurements were carried out. Fig. 5 shows the TPR consumption profiles of methane vs. temperature. As seen, an unique reduction process appears in the temperature range 310-350 °C which can be mainly ascribed to the bulk reaction of PdO to metallic palladium by CH_4 according to the following equation $CH_4 + 4O_{PdO_x} \rightarrow CO_2 + 2H_2O$ as reported elsewhere [34]. Interestingly, methane consumption occurs more readily on Pd/Al-Ce(550) exhibiting the lowest PdO crystallite size, i.e. 1.9 nm and a larger interface at least in comparison with Pd/Al-Ce(950) in agreement with HRTEM observations. At this stage, it seems not easy to formally explain the effect of the calcination temperature on the shift observed on the methane consumption vs. temperature. The delay observed on samples calcined at increasing temperature could be jointly related to changes in the structural properties of CeO_2 as well as on the crystallite size of PdO. As observed in Table 1, the growth observed on CeO_2 and

PdO crystallites size with a rise in calcination temperature could induce a deterioration of the Pd-Ce interaction and then delay this reduction process.

3.2. Textural properties and elemental surface composition

3.2.1. Nitrogen physisorption

Textural analysis from nitrogen physisorption at -196°C leads to same type of isotherms IV for all calcined catalysts [35] corresponding to a monomodal mesopore size distribution exhibiting an apparent maximum near 5.5 nm (Fig. S4 in Supplementary Material). Besides, the pore volume was almost constant. It can be also seen that the BET surface area decreases slightly from 131.9 to 115.0 m^2/g (see Table 1) during the preparation process. This observation shows that the calcination temperature only weakly alters the textural properties which seems in rather good agreement with the moderate growth of CeO_2 crystallite estimated from XRD analysis.

3.2.2. XPS analysis

To unravel the initial Pd species and elemental surface composition over Pd/Al-Ce(x) catalysts, XPS measurements were performed on calcined samples and then pre-activated at 500°C in the reaction mixture to evaluate the impact of this pre-treatment on the oxidation state and the surface composition of palladium. Recording time of spectra was the same for all the samples. Particular attention was paid to Pd 3d and Ce 3d core levels. The deconvolution of Pd 3d and Ce 3d photopeaks was performed by fitting a Gaussian-Lorentzian function. Pd 3d photopeak are shown in Fig. 6. For all calcined catalysts, the photopeaks Pd $3d_{5/2}$ and Pd $3d_{3/2}$ at 336.1 and 341.3 eV

respectively are assigned to Pd^{2+} predominantly stabilized as PdO [36]. No metallic Pd species corresponding to lower B.E. values is observable even for samples calcined 950°C for which the coexistence of PdO crystallites to Pd^0 has been proven from XRD analysis (see Fig. 1c). First, this observation verifies the absence of significant *in situ* surface reduction/decomposition process under X-ray beam exposure. Regarding, the bulk detection of metallic Pd^0 species on samples calcined at high temperature, TPO experiments suggest an incomplete re-oxidation of large metallic Pd particles during the cooling period then preserving a bulk detectable metallic Pd core structure as reported elsewhere [37]. In fact, the absence of detection of metallic Pd species from XPS contrarily to XRD can be easily explained by information obtained at different depth of analysis from nanometer to micrometer respectively. Typically the depth of analysis for XPS, from 2 to 10 nm, is limited by the inelastic means free path of electrons in matter emitted under X-ray bean irradiation depending on the kinetic energy of the electron and the matrix in which the element is located [38]. Therefore, the difference of penetration depth regarding these two techniques (Fig. 1c and Fig. 6) could reasonably explain the lack of detection of metallic Pd species from XPS analysis.

XPS analysis on pre-activated samples reveals different spectral features as exemplified in Table 3. In that case, broader Pd $3d_{5/2}$ can be observed with a growth of a lower B.E. contribution near 335.0 eV characteristic of metallic Pd coexisting with PdO (see Fig. 7). It is remarkable that this low B.E. contribution intensifies with a decreasing Pd particle size. It is noticeable that a slight shift to higher B.E. ascribed to Pd^{2+} is distinguishable on Pd/Al-Ce(550) (~0.7 eV) which could be reasonably explained by a particle-size-induced effect [39]. A similar tendency was previously reported in the work of H. Widjaja et al. [39], who found that the B.E. corresponding

to PdO gradually increased with decreasing the particle size of PdO supported on alumina. Additionally, the relative surface concentrations of Pd and Ce show a decreased trend with increasing Pd size. This suggests a loss of Pd and Ce dispersion onto alumina at increasing calcination temperature, in line with XRD analysis. Generally, the higher the dispersion of Pd and Ce, the more active sites may be provided for the reaction of CH_4 conversion [40, 41].

To determine the relative concentration of metallic Pd and PdO species, the semi-quantitative analysis accounted for a nonlinear Shirley background subtraction with the help of the CasaXPS software. Fig. 7 showed the relationship between the ratio of surface $Pd^0/(Pd^0 + PdO)$ and Pd particle size. Table 3 summarizes the fraction of surface Pd^0 and Ce^{3+} over the catalysts before and after pre-activation in the reaction mixture. It can be clearly seen that the main Pd species over the surface catalysts transformed from PdO to Pd^0 after pre-activation and that Pd/Al-Ce(550) catalyst has the highest surface Pd^0 fraction (87%). On the contrary, Pd/Al-Ce(950) owns the lowest surface Pd^0 fraction (52%). The results indicate that the smaller the Pd particle size, the more likely it is to present a high concentration of active Pd^0 species during the activation process. Additionally, the fraction of surface Ce^{3+} was calculated on calcined samples after decomposition of the Ce 3d photopeak as illustrated in Fig. S5 in Supplementary Material. Pre-activation thermal treatment slightly increases the fraction of surface Ce^{3+} for each catalyst especially on Pd/Al-Ce(550) exhibiting the highest fraction of surface Ce^{3+} (~25%) species. It is generally recognized that the presence of Ce^{3+} is related to the formation of oxygen vacancy [42]. The oxygen vacancy can also act as nucleation centers, promoting the dispersion of the catalysts active phase and thereby enhancing the catalytic activity [43].

3.2.3. Metal dispersion and CO interaction with Pd through in situ DRIFT analysis

In order to get more insight into the calcination temperature dependency of Pd dispersion and average particle size, CO chemisorption measurements were performed. Previous investigations shown that H_2 titration it not trivial because H_2 spill-over effect leading to inaccurate metal dispersion must be prevented [44]. CO Chemisorption experiments were preferred in this study. They were performed at -78°C to suppress CO adsorption on the support [25,26]. As aforementioned, the palladium dispersion was calculated from the amount of adsorbed carbon monoxide assuming CO/Pd = 1 [27]. As seen in Table 1, the dispersion decreases from 0.41 to 0.12 with a rise in calcination temperature from 550 to 950 °C. The average Pd particle size (d_{Pd}) can be roughly estimated from Pd dispersion (D_{Pd}) assuming spherical particle shapes which gave a volume-surface average diameter of d_{Pd} (nm) $=(6 \times 10^5 \times M_{Pd})/ \rho_{Pd} \times S_{Pd} \times D_{Pd}(\%)$ where ρ_{Pd} was the Pd density (12 g/cm^3), M_{Pd} was the the Pd atomic weight (106.4 g/mol), and S_{Pd} was the Pd metal molar surface area (47,8 m^2/mol) [45]. Therefore, the estimated Pd particle sizes in Table 1 increase from 2.7 to 9.2 nm at increasing calcination temperature in rather good agreement with STEM analysis.

The interaction between Pd and Ce is known to induce drastic changes on the catalytic activity [43]. According to the literature [14, 46], the strong metal-support interaction induced by close contact between Pd and Ce can reshape the Pd particles leading to change in the degree of coordination of surface metal Pd atoms. To this end, *in situ* DRIFT measurements during CO adsorption can provide useful information. As shown in Fig. 8a, broad spectra were obtained with apparent maxima arisen in the wavenumber range 1750-2100 cm^{-1}. The 2069 cm^{-1} IR absorption band can be mainly ascribed to linear CO adsorbed onto Pd atoms on corners with low

coordination numbers or on Pd(111) facets [47]. The IR band near 1970 cm^{-1} is currently assigned to bridged CO species adsorbed Pd (100) or Pd (111) facet [48]. Finally, the broad absorption band in the range 1940–1750 cm^{-1} has been attributed to CO adsorbed on hollow sites of Pd (111) facet [49]. Among the catalysts, the strongest peak intensity of the linear and bridged CO adsorbed onto Pd (111) and Pd (100) were observed on Pd/Al-Ce(550) consistent with its best Pd dispersion. As also presented in Fig. 8b, linearly CO species coordinated onto Pd (111) was observed near 2067 cm^{-1} over Pd/Al-Ce(550) corresponding to the lowest average particle size from CO titration. A continuous shift to higher wavenumber values is discernible reaching 2077 cm^{-1} on Pd/Al-Ce(950) corresponding to the largest Pd particles [50].

IR data fitting by using a Gaussian function led to the identification of different components at 2069, 1970, and 1940-1750 cm^{-1}. Spectral decomposition permits a rough estimation of the relative distribution of metallic Pd atoms having low coordination (2069 cm^{-1}) compared to bridged and multi-coordinated CO species appearing at lower wavenumber. The values of the intensity ratio I_{2069}/I_{Total} corresponding to the relative population of linearly coordinated CO species on Pd^0 are reported in Table S1 in Supplementary Material. In case of strong metal-support interaction these low coordination atoms could closely interact with ceria at the periphery of Pd particles. Fig. 9 shows an acceptable correlation between metallic Pd dispersion, I_{2069}/I_{Total} and particle size.

3.3. Kinetics analysis and comparison with surface properties

Catalytic properties of calcined samples from temperature-programmed reaction are reported in Fig. S6 in Supplementary Material. The following sequence of activity in

methane conversion can be established: Pd/Al-Ce(950) < Pd/Al-Ce(900) < Pd/Al-Ce(850) < Pd/Al-Ce(800) < Pd/Al-Ce(550). Similar catalytic features are noticeable when the catalyst is pre-activated in the reaction mixture at 500°C as exemplified in Fig. 10. However, it seems obvious that the onset conversion of methane starts at lower temperature emphasizing better catalytic performances when PdO_x is *in situ* reduced in the course of the pre-activation thermal treatment. The beneficial effect of such pre-treatment has been earlier reported especially on commercial TWC catalysts dedicated to after-treatment of exhaust from natural gas fueled engines [51]. Such beneficial effect could be equally related to a cooperative effect involving a close proximity between Pd and PdO_x or to the involvement of the Pd-Ce interface to activate the dissociative adsorption of methane recognized as the rate determining step for methane oxidation. As shown in Fig. 10a, two kinetic regimes are distinguishable: At low temperature CH_4 conversion gradually increases and does not coincide to NO conversion which underlines that methane is essentially oxidized to CO_2, afterwards a discontinuity appears with a rise in temperature corresponding to a much faster CH_4 conversion jointly with a fast NO conversion (Fig. S7b in Supplementary Material). Accordingly, the reduction of NO would be promoted above 400°C in the presence of methane but the direct reduction of NO by CH_4 would not be the main catalytic process. Indeed, useful information come from the examination of the CO conversion profiles which declines at high temperature suggesting an extra CO production from partial oxidation and/or methane reforming reactions. Hence, it seems more probable that CO and H_2 would act as reducing agent to convert NO more readily instead of methane. It is remarkable that the rate of NO conversion sharply increases when Pd particle size decreases and this tendency also appears for the production of CO which clearly occurs more readily on Pd/Al-Ce(550).

Accordingly, the same trends are observed regarding the beneficial effect of low calcination temperature on the performance of Pd/Al-Ce especially when the catalysts are initially pre-activated in the reaction conditions irrespective of the chemical process involved. Based on this observation, particular attention was paid to the low temperature methane conversion. In this temperature range, methane is predominantly oxidized to CO_2. To further unravel the differences of CH_4 conversion activity associated with different Pd size, kinetic data for CH_4 elimination (Figs. S8 in Supplementary Material and 10b) was determined. Previous verifications showed that in these operating conditions heat and mass transfer phenomena should not occur significantly below 15% methane conversion [27, 52, 53]. Turn-Over-Frequency (TOF) and apparent activation energy values (E_a) from the slope of the Arrhenius plot were also estimated. As seen in Table 4, both specific rates and TOF values increase according to the following sequence Pd/Al-Ce(950) < Pd/Al-Ce(900) < Pd/Al-Ce(850) < Pd/Al-Ce(800) < Pd/Al-Ce(550) which suggests that small metallic Pd particles would be a priori more active than larger ones. Notably, the TOF measured at 340 °C decreased from 0.0119 to 0.0043 s^{-1} as Pd particle size increases from 1.9 to 8.5 nm and the same tendency is also verified at 350 °C. This evolution corresponds to an increase in the apparent activation energy (E_a) from 66.0 to 89.3 $kJmol^{-1}$ slightly lower than those reported in the literature [54]. Fig. 11 provides a good correlation between TOF values and the concentration of surface metallic Pd. Nevertheless, this correlation opens the debate on the real composition of active sites which could not be simply composed of clusters of metallic Pd atoms but could correspond to the creation of active centers at the metal-support interface combining Pd^0 and anionic vacancies. Indeed, previous controversial observations have been reported on Pd/Al_2O_3 showing an optimal Pd particle in the range 1.5-22 nm corresponding to the

highest CH_4 oxidation activity. On the other hand the lowest catalytic activity was obtained on the smallest Pd particles, i.e. 1.5 nm [18]. Despite, these results were obtained in lean conditions 0.5 vol.% CH_4 + 9.0 vol. % O_2 and on different stabilized surfaces with the predominance of PdO, this apparent contradiction suggests that the composition of the support could be a crucial parameter in determining the nature of the active sites.

3.4. General assessment

The investigation clearly shows that the catalytic properties of Pd/Al-Ce will be determined by the calcination temperature leading on pre-activated catalysts, i.e. after exposure to stoichiometric reaction mixture at 500 °C, to the stabilization of oxidic and reduced palladium species and significant changes on particle sizes measured from STEM and CO titration. Clearly the best catalytic performances were obtained on Pd/Al-Ce calcined at 550 °C which reduces more extensively in the course of the pre-activation treatment and correspond to the smallest Pd particle sizes. Let us note that the continuous decrease of specific and TOF values at increasing particle size (see Table 4) differs from the volcano type curves previously discussed [18] revealing optimal particle size on Pd/Al_2O_3 which points out the potential role played by the support through the creation of new active sites at the metal-support interface. XPS analysis also provides additional key information through the calculation the $Ce^{3+}/Ce^{4+}+Ce^{3+}$ ratio. A significant stabilization of Ce^{3+} is usually observed on Pd/Al-Ce irrespective of the pre-treatment, i.e. calcination or pre-activation in reaction mixture, which can be associated to the more extensive stabilization of anionic vacancies coming from more labile oxygen species. Based on

these observations the promotional effect observed after pre-treatment of the Pd/Al-Ce(550) could be related to the cooperation of metallic Pd atoms at the vicinity of anionic vacancies and/or surface reactive labile oxygen species. A rise in calcination temperature on Pd/Al-Ce(950) has a strong detrimental effect on the catalytic properties. Several factors could explain this loss of performance related to the growth of Pd particles and CeO_2 crystallite as evidence from STEM, CO chemisorption and XRD measurements (see Table 1). In such conditions the cooperative effect of Pd and ceria would be deteriorated likely due to a lower interfacial perimeter as well as an alteration of oxygen mobility. Accordingly, the cooperation of Pd and PdO could become predominant with oxygen supplied by PdO instead of ceria. Such an explanation has been earlier privileged and the lower activity previously obtained on Pd/Al_2O_3 has been ascribed to a stronger Pd–O bond which was supposed to decrease oxygen mobility in Pd oxide species, thereby leading to a lower specific activity for CH_4 oxidation [48]. As a matter of fact, earlier investigations shown that the presence of surface oxygen species favor the hydrogen abstraction from CH_4 and/or adsorbed CH_x species [55-58]. On the basis of these findings, the variation observed on the TOF could reflect a change in kinetic regime where assisted dissociation of methane on metallic Pd species would be no longer favored by a nearest neighbor oxygen species from ceria but would occur more slowly thanks to less labile oxygen coming from PdO.

Earlier investigation highlighted the specific role played by the metal-support interface through the calculation of interfacial rate taking the length of the perimeter of the Pt–support interface (μmol cm^{-1} s^{-1}) [59, 60]. The perimeter of metallic Pd particles l_0 (cm/g) can be roughly estimated accounting for particles with a circular geometry at the interface and the Pd density ρ_{Pd} = 12.02 $g.cm^{-3}$. This calculation agrees with the

fact that the density of oxygen atoms from ceria adjacent to metallic Pd sites is dependent of the Pd particles. The obtained values for l_0 oscillate in the range (6.9-139)$\times 10^{11}$ cm.g^{-1} leading to interfacial rates expressed per cm in Table 4. In practice, the comparison of TOF and interfacial rates can lead to the isolation of different kinetic regimes as earlier found especially in the particular case of structure-sensitive reaction [59]. By way of illustration Wu et al. [59] found that NO reduction by H_2 on Pt/$LaFeO_3$ becomes structure-insensitive when the kinetics is governed by the metal-support interface. On the other hand, the structure sensitivity is restored when the Pt-support interface is deteriorated. Returning to methane conversion these two borderlines cases do not appear distinctly in Fig. 12. As a matter of fact, the comparison observed on TOF and interfacial rate predominantly underlines a mixed kinetic regimes with at the extremes a significantly different kinetic behavior. By examining the kinetic behavior for small and large Pd particle sizes the slopes of the corresponding straight lines for the plot interfacial rate vs Pd particle size clearly shows that the interface should predominate for small particles whereas the weaker slope observed for large particles underlines a lessened contribution corresponding to slightly lower TOF values. As already mentioned these kinetic features match correctly with a significant increase in the apparent activation energy. Accordingly, these deviations are consistent with the coexistence of two different active centers at the interface for small Pd particles through the assistance of oxygen from ceria to dissociate methane whereas for large particles active oxygen from PdO could assist methane activation corresponding to a lower TOF due to a stronger Pd-O bond.

The implementation of Density Functional Theory (DFT) complemented experimental approaches especially to clarify the role of oxygen to activate methane on model surfaces [61, 62]. Literature data can provide some controversies regarding the

nature of oxygen which originates rate enhancement in methane conversion. Beneficial effects have been reported by Wang et al. [63] whereas Valden et al. [64, 65] found a detrimental effect of pre-covered oxygen Pd(110) and Pd(111) surfaces. These authors concluded that high oxygen coverage induces strong inhibition of the dissociative adsorption of methane. Time-resolved *in situ* XANES spectroscopy and DFT modeling found that intermediate O/Pt ratio is more favorable to get optimal activity and also verified that oxygen-rich surface would prevent the dissociative adsorption of methane [66] Interestingly, lower activation barrier were reported on $Pd_xCe_{1-x}O_2$(111) [67] in comparison with Pd(111) and pre-covered PdO(111) explained by enhanced OSC properties if ceria closely interact with palladium. In this specific case oxygen spill-over from metallic Pt sites refilling anionic vacancies could prevent strong oxygen inhibiting effect. Consequently, all the kinetics features recorded on Pd/Al-Ce could be also reconciled if changes observed on the apparent activation energy could be related to a strengthening of the oxygen inhibiting effect at increasing particle size jointly related to a loss of the metal-support interaction.

Let us note that this explanation can also rationalize the rate enhancement observed on the reduction of NO recognized as structure-sensitive because two nearest-neighbor vacant site is needed for NO dissociation. Hence, the development of the Pd-Ce interface could minimize the oxygen inhibition preserving a significant probability to find a pair of empty sites. Alternately, the creation of dual sites at the periphery of Pd particles offers the possibility of adsorbed NO on Pd to dissociate on a nearest-neighbor anionic vacancy. All these observations emphasize the key role played by the Pd-Ce interface which outperforms the performance induced by the Pd-PdO interaction when the Pd-Ce interface becomes deteriorated at high temperature.

4. Conclusions

This study dealt with the impact of the calcination temperature on the pre-activation thermal treatment of Pd/Al_2O_3-CeO_2 NGV catalysts. The investigation of the catalytic properties of preactivated catalysts took practical issues into consideration. Indeed, washcoated monolith catalysts have been studied in real exhaust gas stoichiometric composition. Particular attention was paid to the abatement of methane emissions at low temperature among the other atmospheric pollutants such as NO and CO. Two kinetic regimes vs. calcination temperature were characterized from the calculation of TOF, interfacial rate and apparent activation energy corresponding to PdO_x crystallite exhibiting different reducibility. Optimal catalytic properties were obtained in stoichiometric conditions on samples calcined at the lowest temperature, i.e. 550°C, corresponding to the generation of small metallic Pd particles. The monitoring of small Pd^0 particle sizes may be helpful for the development of highly efficient Pd catalysts for CH_4 elimination. But the indispensable interaction with ceria was proven showing that the related performance outperformed those obtained resulting from Pd-PdO interaction when the Pd-Ce interface is degraded at high calcination temperature. Indeed, the assistance of oxygen to facilitate methane dissociation would be governed by the higher mobility of oxygen from ceria instead of PdO. All these kinetic features also match to explain the rate enhancement in NO reduction likely due to a much faster dissociation of NO at the vicinity of anionic vacancies then refilled.

This lab-scale study could open new guidelines on prerequisites for developing optimized NGV catalysts. Of course, practical developments likely need to explore the catalyst stability under more severe conditions and periodic conditions. Let us

note that new advanced were recently obtained in our lab revealing on this variety of catalyst the absence of palladium particle sintering on Pd/Al-Ce(550) in periodic conditions which could be considered as a good starting point for future practical investigations pointing out the importance of the stabilizing effect of ceria in interaction with nano-sized metallic Pd particles.

Acknowledgement

This work was supported by the National Key R&D Program of China (2016YFC0204902), the National Natural Science Foundation of China (21673146), the Graduate Student's Research and Innovation Fund of Sichuan University (2018YJSY093), and the Doctoral Graduate Students' Academic Visit Fund of Sichuan University. We also thank the Yunfei Tian of the Analytical & Testing Center of Sichuan University for XPS work and Shanling Wang of the Analytical & Testing Center (ATC) of Sichuan University for performing TEM characterization.

References

[1] P. Granger, Challenges and breakthroughs in post-combustion catalysis: how to match future stringent regulations, Catal. Sci. Technol. 7 (2017) 5195-5211. http://doi.org/ 10.1039/c7cy00983f.

[2] D. Ferri, M. Elsener, O. Kröcher, Methane oxidation over a honeycomb Pd-only three-way catalyst under static and periodic operation, Appl. Catal., B 220 (2017) 67-77. http://doi.org/ 10.1016/j.apcatb.2017.07.070.

[3] N. Sadokhina, G. Smedler, U. Nylén, M. Olofsson, L. Olsson, The influence of gas composition on Pd-based catalyst activity in methane oxidation – inhibition and promotion by NO, Appl. Catal., B 200 (2017) 351-360. http://doi.org/ 10.1016/j.apcatb.2016.07.012.

[4] M. Cargnello, J.J. Delgado Jaen, J.C. Hernandez Garrido, K. Bakhmutsky, T. Montini, J.J. Calvino Gamez, R.J. Gorte, P. Fornasiero, Exceptional activity for methane combustion over modular Pd@CeO2 subunits on functionalized Al_2O_3, Science 337 (2012) 713-717. http://doi.org/ 10.1126/science.1222887.

[5] A. Raj, Methane Emission Control, Johnson Matthey Technol. Rev. 60 (2016) 228-235. http://doi.org/ 10.1595/205651316X692554.

[6] G. Beulertz, M. Votsmeier, R. Moos, Effect of propene, propane, and methane on conversion and oxidation state of three-way catalysts: a microwave cavity perturbation study, Appl. Catal., B 165 (2015) 369-377. http://doi.org/ 10.1016/j.apcatb.2014.09.068.
[7] H. Xiong, M.H. Wiebenga, C. Carrillo, J.R. Gaudet, H.N. Pham, D. Kunwar, S.H. Oh, G. Qi, C.H. Kim, A.K. Datye, Design considerations for low-temperature hydrocarbon oxidation reactions on Pd based catalysts, Appl. Catal., B 236 (2018) 436-444. http://doi.org/ 10.1016/j.apcatb.2018.05.049.
[8] F. Huang, J. Chen, W. Hu, G. Li, Y. Wu, S. Yuan, L. Zhong, Y. Chen, Pd or PdO: Catalytic active site of methane oxidation operated close to stoichiometric air-to-fuel for natural gas vehicles, Appl. Catal., B 219 (2017) 73-81. http://doi.org/ 10.1016/j.apcatb.2017.07.037.
[9] M. Monai, T. Montini, R.J. Gorte, P. Fornasiero, Catalytic Oxidation of Methane: Pd and Beyond, Eur. J. Inorg. Chem. (2018) 2884-2893. http://doi.org/ 10.1002/ejic.201800326.
[10] S. Subramanian, R.J. Kudla, M.S. Chattha, Removal of methane from compressed natural gas fueled vehicle exhaust, Ind. Eng. Chem. Res. 31 (1992) 2460-2465. http://doi.org/ 10.1021/ie00011a009.
[11] P. Munnik, P.E. de Jongh, K.P. de Jong, Recent developments in the synthesis of supported catalysts, Chem Rev 115 (2015) 6687-6718. http://doi.org/ 10.1021/cr500486u.
[12] J.J. Willis, A. Gallo, D. Sokaras, H. Aljama, S.H. Nowak, E.D. Goodman, L. Wu, C.J. Tassone, T.F. Jaramillo, F. Abild-Pedersen, M. Cargnello, Systematic Structure-Property Relationship Studies in Palladium-Catalyzed Methane Complete Combustion, ACS Catal. 7 (2017) 7810-7821. http://doi.org/ 10.1021/acscatal.7b02414.
[13] P. Gélin, M.P. , Complete oxidation of methane at low temperature over noble metal based catalysts: a review, Appl. Catal., B 39 (2002) 1-37. http://doi.org/ 10.1016/S0926-3373(02)00076-0.
[14] D. Ciuparu, M.R. Lyubovsky, E. Altman, L.D. Pfefferle, A. Datye, Catalytic Combustion of Methane over Palladium-Based Catalysts, Catal. Rev. 44 (2002) 593-649. http://doi.org/ 10.1081/cr-120015482.
[15] C. Carrillo, H. Xiong, A.T. DeLaRiva, D. Kunwar, E.J. Peterson, S.R. Challa, G. Qi, S. Oh, M.H. Wiebenga, X.I.P. Hernandez, Y. Wang, A.K. Datye, Designing Catalysts for Meeting the DOE 150 °C Challenge for Exhaust Emissions, Microscopy and Microanalysis 23 (2017) 2028-2029. http://doi.org/ 10.1017/s1431927617010807.
[16] S.B. Kang, J.B. Lim, D. Jo, I.-S. Nam, B.K. Cho, S.B. Hong, C.H. Kim, S.H. Oh, Ostwald-ripening sintering kinetics of Pd-based three-way catalyst: Importance of initial particle size of Pd, Chem. Eng. J. 316 (2017) 631-644. http://doi.org/ 10.1016/j.cej.2017.01.136.
[17] H.Q. Robert F. Hicks, Michael L.Young, Raymond G.Lee, Structure Sensitivity of Methane Oxidation over Platinum and Pd, J. Catal. 122 (1990) 280-294. http://doi.org/ 10.1016/0021-9517(90)90282-O.
[18] A.Y. Stakheev, A.M. Batkin, N.S. Teleguina, G.O. Bragina, V.I. Zaikovsky, I.P. Prosvirin, A.K. Khudorozhkov, V.I. Bukhtiyarov, Particle Size Effect on CH_4 Oxidation Over Noble Metals: Comparison of Pt and Pd Catalysts, Top. Catal. 56 (2013) 306-310. http://doi.org/ 10.1007/s11244-013-9971-y.
[19] K.-I. Fujimoto, F.H. Ribeiro, M. Avalos-Borja, E. Iglesia, Structure and reactivity of PdO_x/ZrO_2Catalysts for methane oxidation at low temperatures, J. Catal. 179 (1998) 431-442. http://doi.org/ 10.1006/jcat.1998.2178.
[20] J.H. Guanghui Zhu, Dmitri Y. Zemlyanov, Fabio H. Ribeiro, The Turnover Rate for the Catalytic Combustion of Methane over Palladium Is Not Sensitive to the Structure of the Catalyst, J Am Chem

Soc 126 (2004) 9896-9897. http://doi.org/ 10.1021/ja049406s.
[21] F. Ribeiro, M. Chow, R. Dallabetta, Kinetics of the complete oxidation of methane over supported palladium catalysts, J. Catal. 146 (1994) 537-544. http://doi.org/ 10.1006/jcat.1994.1092.
[22] D. Bounechada, G. Groppi, P. Forzatti, K. Kallinen, T. Kinnunen, Effect of periodic lean/rich switch on methane conversion over a Ce–Zr promoted Pd-Rh/Al_2O_3 catalyst in the exhausts of natural gas vehicles, Appl. Catal., B 119-120 (2012) 91-99. http://doi.org/ 10.1016/j.apcatb.2012.02.025.
[23] J. Chen, Y. Wu, W. Hu, P. Qu, G. Zhang, Y. Jiao, L. Zhong, Y. Chen, Evolution of Pd Species for the Conversion of Methane under Operation Conditions, Ind. Eng. Chem. Res. 58 (2019) 6255-6265. http://doi.org/ 10.1021/acs.iecr.8b06226.
[24] J. Chen, W. Hu, F. Huang, Y. Wu, S. Yuan, L. Zhong, Y. Chen, P promotion on the performance of Pd-based catalyst for emission control of natural gas driven vehicles, J. Taiwan. Inst. Chem. E. 91 (2018) 323-331. http://doi.org/ 10.1016/j.jtice.2018.05.037.
[25] M. Hatanaka, N. Takahashi, T. Tanabe, Y. Nagai, K. Dohmae, Y. Aoki, T. Yoshida, H. Shinjoh, Ideal Pt loading for a Pt/CeO_2-based catalyst stabilized by a Pt–O–Ce bond, Appl. Catal., B 99 (2010) 336-342. http://doi.org/ 10.1016/j.apcatb.2010.07.003.
[26] Y. Nagai, T. Hirabayashi, K. Dohmae, N. Takagi, T. Minami, H. Shinjoh, S. Matsumoto, Sintering inhibition mechanism of platinum supported on ceria-based oxide and Pt-oxide–support interaction, J. Catal. 242 (2006) 103-109. http://doi.org/ 10.1016/j.jcat.2006.06.002.
[27] D.Y. Yoon, Y.J. Kim, J.H. Lim, B.K. Cho, S.B. Hong, I.-S. Nam, J.W. Choung, Thermal stability of Pd-containing $LaAlO_3$ perovskite as a modern TWC, J. Catal. 330 (2015) 71-83. http://doi.org/ 10.1016/j.jcat.2015.07.013.
[28] A.K. Datye, J. Bravo, T.R. Nelson, P. Atanasova, M. Lyubovsky, L. Pfefferle, Catalyst microstructure and methane oxidation reactivity during the Pd↔PdO transformation on alumina supports, Appl. Catal., A 198 (2000) 179-196. http://doi.org/ 10.1016/S0926-860X(99)00512-8.
[29] J.R. Anderson, K.C. Pratt, Introduction to characterization and testing of catalysts, Academic Pr1985.
[30] X. Chen, J.W. Schwank, G.B. Fisher, Y. Cheng, M. Jagner, R.W. McCabe, M.B. Katz, G.W. Graham, X. Pan, Nature of the two-step temperature-programmed decomposition of PdO supported on alumina, Appl. Catal., A 475 (2014) 420-426. http://doi.org/ 10.1016/j.apcata.2014.01.056.
[31] J.J. Willis, E.D. Goodman, L. Wu, A.R. Riscoe, P. Martins, C.J. Tassone, M. Cargnello, Systematic Identification of Promoters for Methane Oxidation Catalysts Using Size- and Composition-Controlled Pd-Based Bimetallic Nanocrystals, J Am Chem Soc 139 (2017) 11989-11997. http://doi.org/ 10.1021/jacs.7b06260.
[32] S. Lin, L. Yang, X. Yang, R. Zhou, Redox properties and metal–support interaction of Pd/Ce0.67Zr0.33O2–Al2O3 catalyst for CO, HC and NO_x elimination, Appl. Surf. Sci. 305 (2014) 642-649. http://doi.org/ 10.1016/j.apsusc.2014.03.153.
[33] S. Colussi, A. Trovarelli, G. Groppi, J. Llorca, The effect of CeO_2 on the dynamics of Pd–PdO transformation over Pd/Al_2O_3 combustion catalysts, Catal. Commun. 8 (2007) 1263-1266. http://doi.org/ 10.1016/j.catcom.2006.11.020.
[34] Y. Lou, J. Ma, W. Hu, Q. Dai, L. Wang, W. Zhan, Y. Guo, X.-M. Cao, Y. Guo, P. Hu, G. Lu, Low-Temperature Methane Combustion over Pd/H-ZSM-5: Active Pd Sites with Specific Electronic Properties

Modulated by Acidic Sites of H-ZSM-5, ACS Catal. 6 (2016) 8127-8139. http://doi.org/10.1021/acscatal.6b01801.
[35] K.S.W. Sing, Reporting physisorption data for gas/solid systems with special reference to the determination of surface area and porosity, Pure Appl. Chem. 57 (1985) 603. http://doi.org/10.1351/pac198557040603.
[36] M. Salaün, A. Kouakou, S. Da Costa, P. Da Costa, Synthetic gas bench study of a natural gas vehicle commercial catalyst in monolithic form: On the effect of gas composition, Appl. Catal., B 88 (2009) 386-397. http://doi.org/ 10.1016/j.apcatb.2008.10.026.
[37] J. Nilsson, P.-A. Carlsson, N.M. Martin, E.C. Adams, G. Agostini, H. Grönbeck, M. Skoglundh, Methane oxidation over Pd/Al2O3 under rich/lean cycling followed by operando XAFS and modulation excitation spectroscopy, J. Catal. 356 (2017) 237-245. http://doi.org/ 10.1016/j.jcat.2017.10.018.
[38] J. Chastain, R.C. King, J. Moulder, Handbook of X-ray photoelectron spectroscopy: a reference book of standard spectra for identification and interpretation of XPS data, Physical Electronics Division, Perkin-Elmer Corporation Eden Prairie, Minnesota1992.
[39] H. Widjaja, K. Sekizawa, K. Eguchi, H. Arai, Oxidation of methane over Pd-supported catalysts, Catal. Today 35 (1997) 197-202. http://doi.org/ 10.1016/S0920-5861(96)00128-9
[40] J. Wang, H. Chen, Z. Hu, M. Yao, Y. Li, A Review on the Pd-Based Three-Way Catalyst, Catal. Rev. 57 (2014) 79-144. http://doi.org 10.1080/01614940.2014.977059.
[41] J.A. Rodriguez, D.C. Grinter, Z. Liu, R.M. Palomino, S.D. Senanayake, Ceria-based model catalysts: fundamental studies on the importance of the metal-ceria interface in CO oxidation, the water-gas shift, CO_2 hydrogenation, and methane and alcohol reforming, Chem Soc Rev 46 (2017) 1824-1841. http://doi.org/ 10.1039/c6cs00863a.
[42] L. Yang, X. Yang, S. Lin, R. Zhou, Insights into the role of a structural promoter (Ba) in three-way catalyst Pd/CeO_2–ZrO_2using in situ DRIFTS, Catal. Sci. Technol. 5 (2015) 2688-2695. http://doi.org/10.1039/c5cy00117j.
[43] T. Montini, M. Melchionna, M. Monai, P. Fornasiero, Fundamentals and Catalytic Applications of CeO_2-Based Materials, Chem Rev 116 (2016) 5987-6041. http://doi.org/ 10.1021/acs.chemrev.5b00603.
[44] S. Bernal, J.J Calvino, G.A. Cifredo, J.M. Rodriguez-Izquierdo, V. Perrichon, A. Laachir, Reversibility of Hydrogen Chemisorption on a Ceria-Supported Rhodium Catalyst, J. Catal. 137 (1992) 1-11. https://doi.org/10.1016/0021-9517(92)90134-4.
[45] A. Baylet, S. Royer, P. Marécot, J.M. Tatibouët, D. Duprez, Effect of Pd precursor salt on the activity and stability of Pd-doped hexaaluminate catalysts for the CH_4 catalytic combustion, Appl. Catal., B 81 (2008) 88-96. http://doi.org/ 10.1016/j.apcatb.2007.12.004.
[46] P. Gélin, M. Primet, Complete oxidation of methane at low temperature over noble metal based catalysts: a review, Appl. Catal., B 39 (2002) 1-37. http://dx.doi.org/10.1016/S0926-3373(02)00076-0.
[47] L. Ding, H. Yi, W. Zhang, R. You, T. Cao, J. Yang, J. Lu, W. Huang, Activating Edge Sites on Pd Catalysts for Selective Hydrogenation of Acetylene via Selective Ga_2O_3 Decoration, ACS Catal. 6 (2016) 3700-3707. http://doi.org/ 10.1021/acscatal.6b00702.
[48] K. Murata, Y. Mahara, J. Ohyama, Y. Yamamoto, S. Arai, A. Satsuma, The Metal-Support Interaction Concerning the Particle Size Effect of Pd/Al_2O_3 on Methane Combustion, Angew. Chem. Int. Edit. 129

(2017) 1-6. http://doi.org/ 10.1002/anie.201709124.
[49] G.S. Zorn K, Halwax E, CO oxidation on technological Pd–Al_2O_3 catalysts: oxidation state and activity, J. Phys. Chem. C 115 (2010) 1103-1111. http://doi.org/ 10.1021/jp106235x.
[50] S. Royer, D. Duprez, Catalytic Oxidation of Carbon Monoxide over Transition Metal Oxides, ChemCatChem 3 (2011) 24-65. http://doi.org/ 10.1002/cctc.201000378.
[51] T. Johnson, A. Joshi, Review of Vehicle Engine Efficiency and Emissions, SAE Technical Paper 2017-01-0907 (2017). http://doi.org/ 10.4271/2017-01-0907.
[52] J.C. Y. Wu, W. Hu, P. Qu, P. Shen, M. Zhao, L. Zhong, Y. Chen, Phase transformation and oxygen vacancies in Pd/ZrO_2 for completed methane oxidation under lean conditions, J. Catal. (2019). Just Accepted.
[53] W. Hu, G.X. Li, J.J. Chen, F.J. Huang, Y. Wu, S.D. Yuan, L. Zhong, Y.Q. Chen, Enhanced catalytic performance of a PdO catalyst prepared via a two-step method of in situ reduction-oxidation, Chem Commun (Camb) 53 (2017) 6160-6163. http://doi.org/ 10.1039/c7cc01997a.
[54] J. Xu, L. Ouyang, W. Mao, X.-J. Yang, X.-C. Xu, J.-J. Su, T.-Z. Zhuang, H. Li, Y.-F. Han, Operando and Kinetic Study of Low-Temperature, Lean-Burn Methane Combustion over a Pd/γ-Al_2O_3Catalyst, ACS Catal. 2 (2012) 261-269. http://doi.org/ 10.1021/cs200694k.
[55] D. Wang, Z. Li, C. Luo, W. Weng, H. Wan, OH spillover from a γ-Al_2O_3 support in the partial oxidation of methane over Ru/Al_2O_3, Chem. Eng. Sci. 58 (2003) 887-893. http://doi.org/ 10.1016/S0009-2509(02)00620-6.
[56] A.M. O'Connor, Y. Schuurman, J.R.H. Ross, C. Mirodatos, Transient studies of carbon dioxide reforming of methane over Pt/ZrO_2 and Pt/Al_2O_3, Catal. Today 115 (2006) 191-198. http://doi.org/ 10.1016/j.cattod.2006.02.051.
[57] Y. Schuurman, C. Marquez-Alvarez, V.C.H. Kroll, C. Mirodatos, Unraveling mechanistic features for the methane reforming by carbon dioxide over different metals and supports by TAP experiments, Catal. Today 46 (1998) 185-192. http://doi.org/ 10.1016/S0920-5861(98)00340-X.
[58] D. Wang, O. Dewaele, A.M.D. Groote, G.F. Froment, Reaction Mechanism and Role of the Support in the Partial Oxidation of Methane on Rh/Al_2O_3, J. Catal. 159 (1996) 418-426. http://doi.org/10.1006/jcat.1996.0105.
[59] Y. Wu, C. Dujardin, C. Lancelot, J.P. Dacquin, V.I. Parvulescu, M. Cabié, C.R. Henry, T. Neisius, P. Granger, Catalytic abatement of NO and N_2O from nitric acid plants: A novel approach using noble metal-modified perovskites, J. Catal. 328 (2015) 236-247. http://doi.org/ 10.1016/j.jcat.2015.02.001.
[60] C.M. Kalamaras, S. Americanou, A.M. Efstathiou, "Redox" vs "associative formate with –OH group regeneration" WGS reaction mechanism on Pt/CeO_2: Effect of platinum particle size, J. Catal. 279 (2011) 287. http://doi.org/ 10.1016/j.jcat.2011.01.024.
[61] B.S. Bunnik, G.J. Kramer, Energetics of methane dissociative adsorption on Rh{111} from DFT calculations, J. Catal. 242 (2006) 309-318. http://doi.org/ 10.1016/j.jcat.2006.06.015.
[62] F. Abild-Pedersen, O. Lytken, J. Engbæk, G. Nielsen, I. Chorkendorff, J.K. Nørskov, Methane activation on Ni(111): Effects of poisons and step defects, Surf. Sci. 590 (2005) 127-137. http://doi.org/ 10.1016/j.susc.2005.05.057.
[63] J.-G. Wang, C.-J. Liu, Density functional theory study of methane activation over PdO/HZSM-5, J.

Mol. Catal. A: Chem. 247 (2006) 199-205. http://doi.org/ 10.1016/j.molcata.2005.11.054.
[64] M. Valden, J. Pere, N. Xiang, M. Pessa, Influence of preadsorbed oxygen on activated chemisorption of methane on Pd(110), Chemical Physics Letters 257 (1996) 289-296. http://doi.org/ 10.1016/0009-2614(96)00554-4.
[65] M. Valden, J. Pere, M. Hirsimäki, S. Suhonen, M. Pessa, Activated adsorption of methane on clean and oxygen-modified Pt{111} and Pd{110}, Surf. Sci. 377-379 (1997) 605-609. http://doi.org/ 10.1016/S0039-6028(96)01462-8.
[66] E. Becker, P.-A. Carlsson, H. Grönbeck, M. Skoglundh, Methane oxidation over alumina supported platinum investigated by time-resolved in situ XANES spectroscopy, J. Catal. 252 (2007) 11-17. http://doi.org/ 10.1016/j.jcat.2007.09.004.
[67] A.D. Mayernick, M.J. Janik, Methane oxidation on Pd–Ceria: A DFT study of the mechanism over $Pd_xCe_{1-x}O_2$, Pd, and PdO, J. Catal. 278 (2011) 16-25. http://doi.org/ 10.1016/j.jcat.2010.11.006.

1

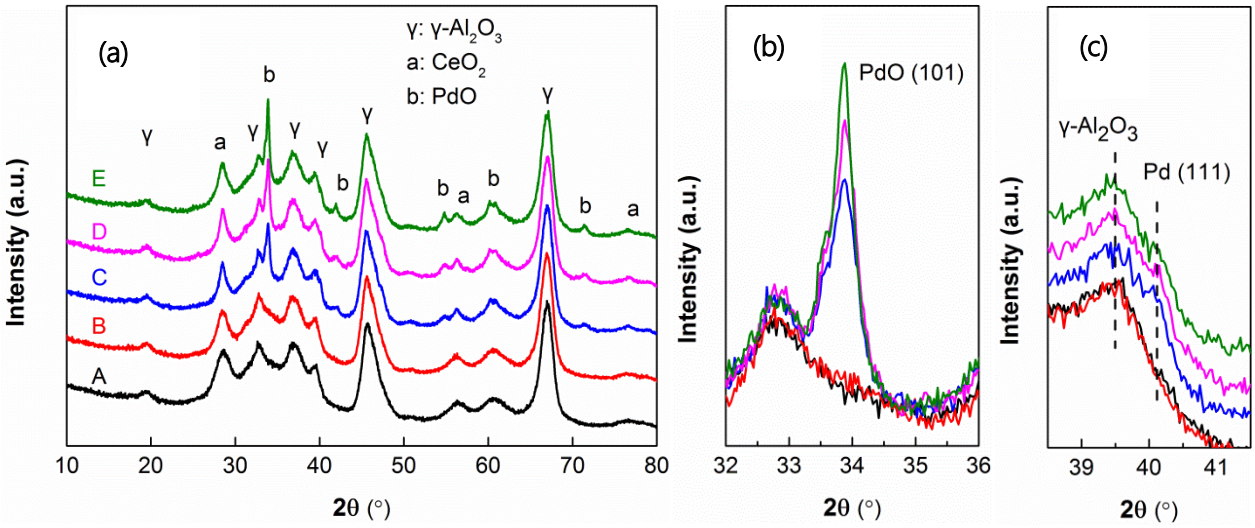

Fig. 1. (a) XRD patterns recorded on calcined Pd/Al-Ce(x) catalysts; (b) amplified diffraction patterns corresponding to PdO (101) and (c) Pd (111) reflections. A: Pd/Al-Ce(550); B: Pd/Al-Ce(800); C: Pd/Al-Ce(850); D: Pd/Al-Ce(900), and E: Pd/Al-Ce(950).

2

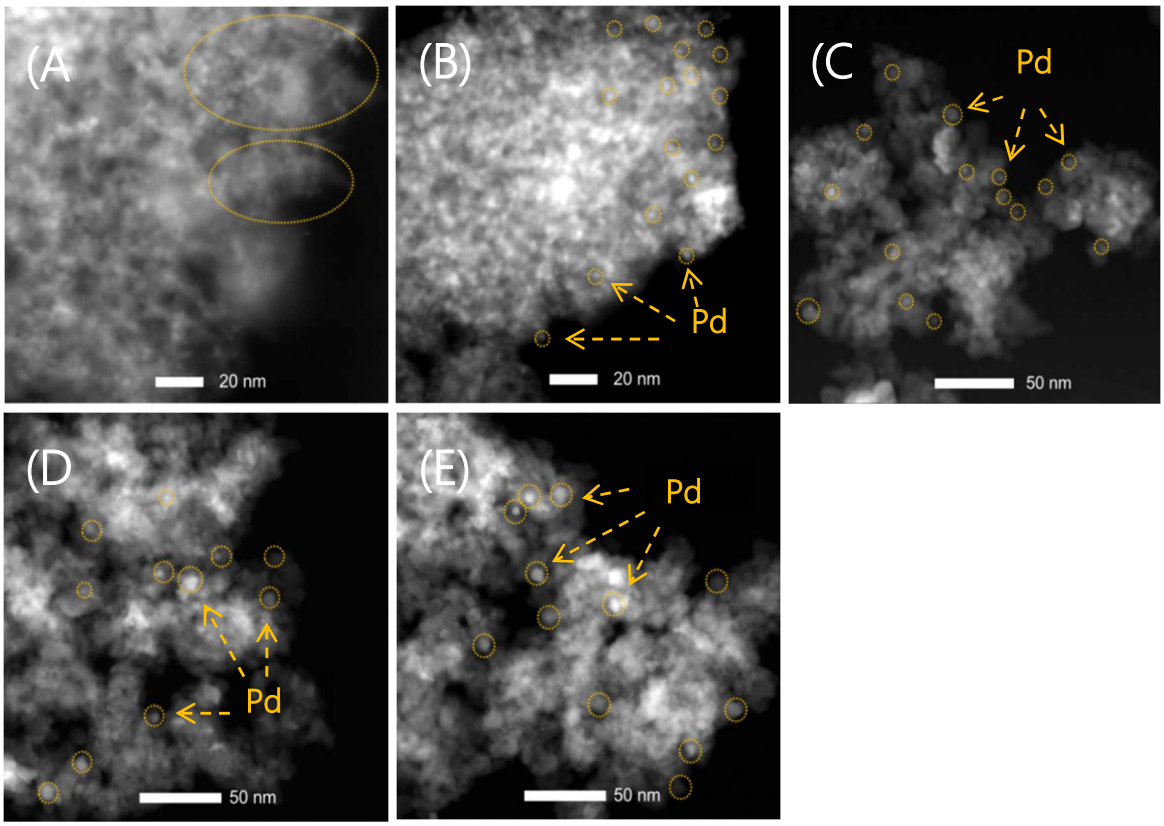

Fig. 2. The STEM images of calcined Pd/Al-Ce(x) catalysts. A: Pd/Al-Ce(550); B: Pd/Al-Ce(800); C: Pd/Al-Ce(850); D: Pd/Al-Ce(900); and E: Pd/Al-Ce(950).

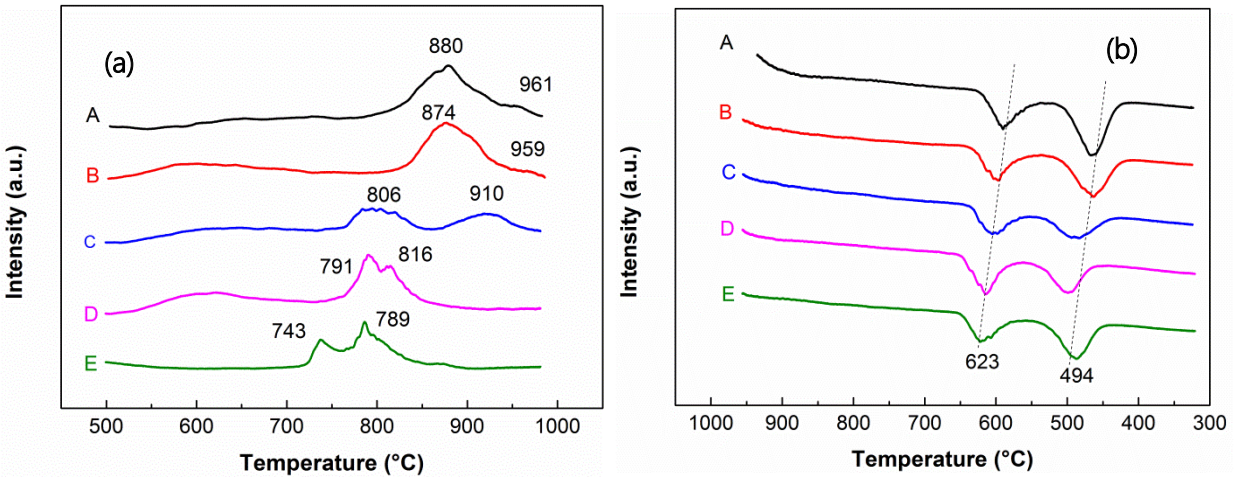

Fig. 3. (a) heating and (b) cooling curves vs. temperature during TPO experiments on calcined Pd/Al-Ce(x) catalysts. Flow rate of 40 mL min^{-1} of O_2 (2%)/Ar. Heating and cooling rates of 10 °C min^{-1}. A: Pd/Al-Ce(550); B: Pd/Al-Ce(800); C: Pd/Al-Ce(850); D: Pd/Al-Ce(900), and E: Pd/Al-Ce(950).

1

2

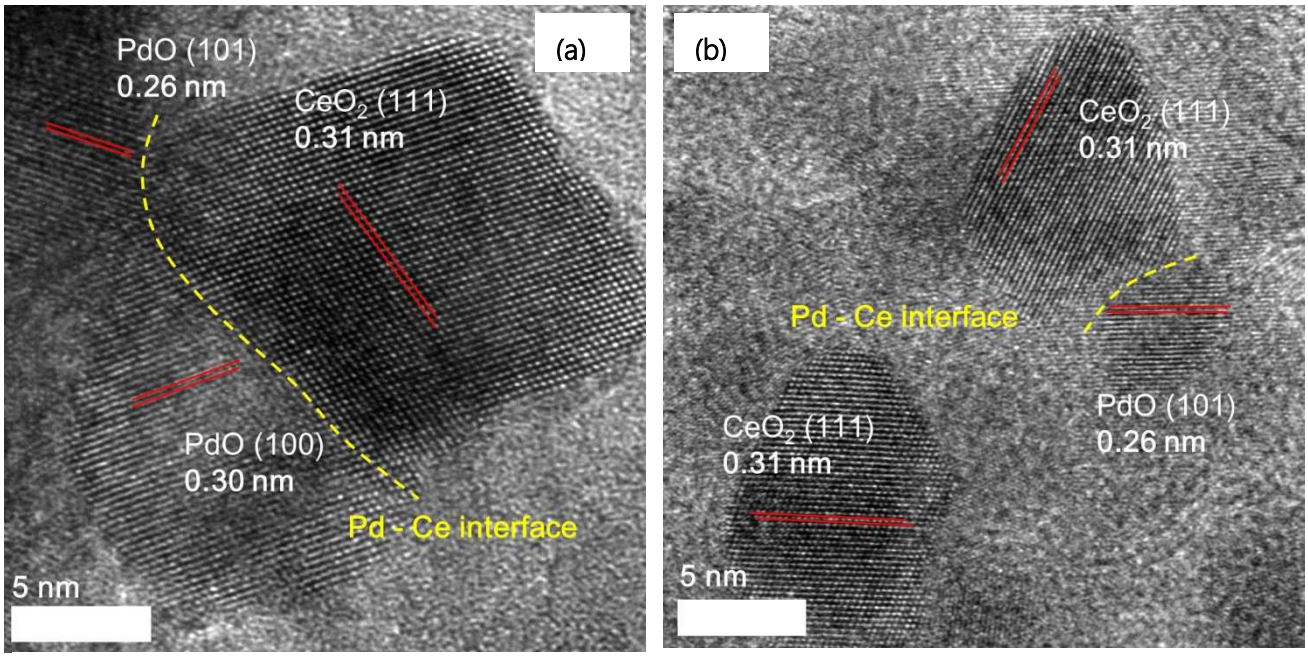

Fig. 4. HRTEM images recorded on: (a) calcined Pd/Al-Ce(550) and (b) Pd/Al-Ce(950) corresponding a larger Pd-Ce interface in the former sample.

3

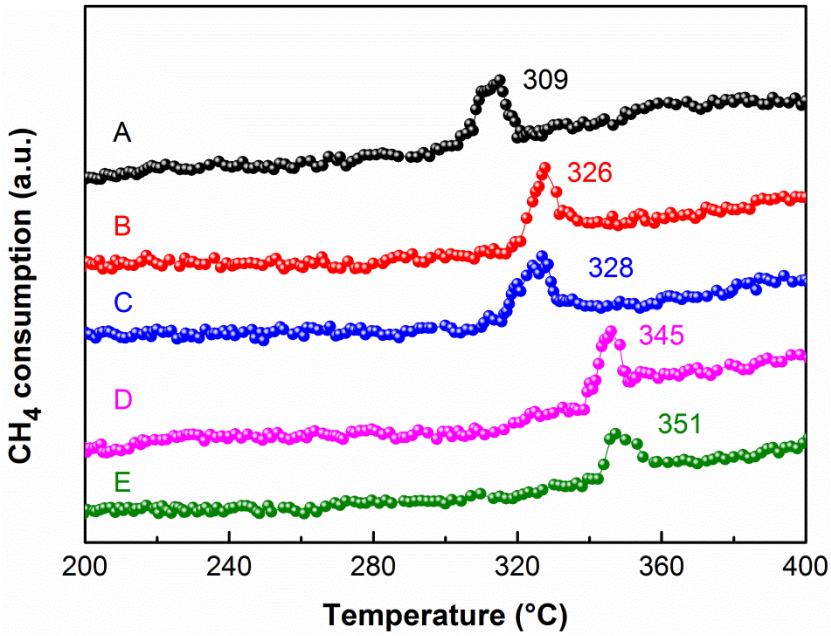

Fig. 5. Methane conversion profiles vs temperature in the course of CH_4-TPR experiments on calcined Pd/Al-Ce(x) catalysts. Flow rate of 50 mL min^{-1} of 1 vol.% CH_4 in Ar. Heating rate of 10 °C min^{-1}. A: Pd/Al-Ce(550); B: Pd/Al-Ce(800); C: Pd/Al-Ce(850); D: Pd/Al-Ce(900) and E: Pd/Al-Ce(950).

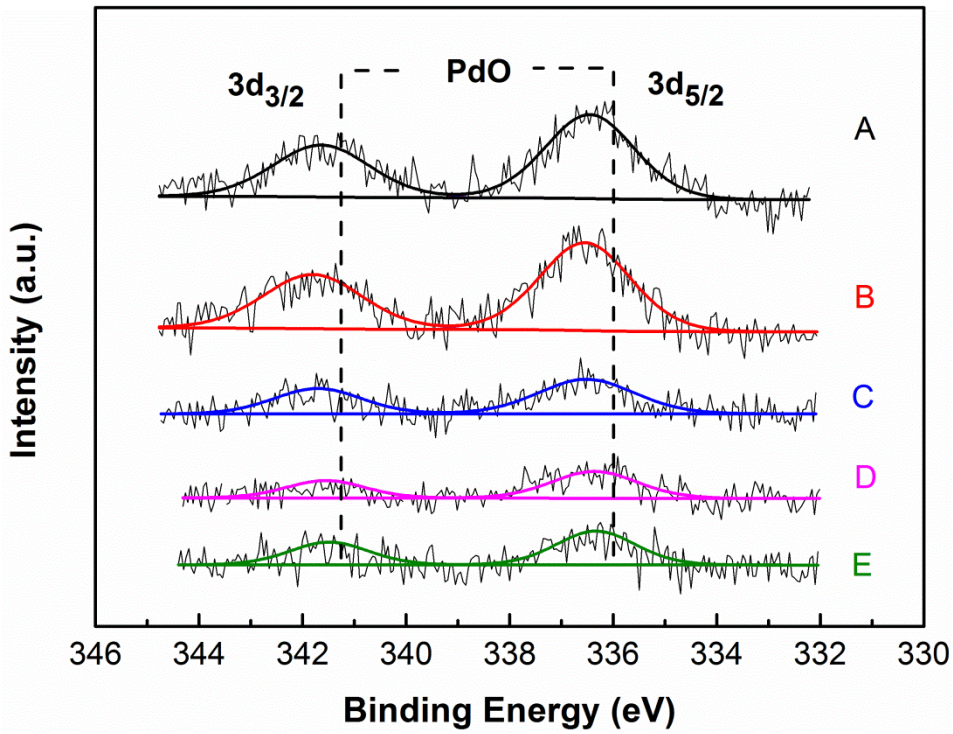

Fig. 6. Pd 3d photopeak recorded on calcined Pd/Al-Ce(x) catalysts before pre-activation. A: Pd/Al-Ce(550); B: Pd/Al-Ce(800); C: Pd/Al-Ce(850); D: Pd/Al-Ce(900) and E: Pd/Al-Ce(950).

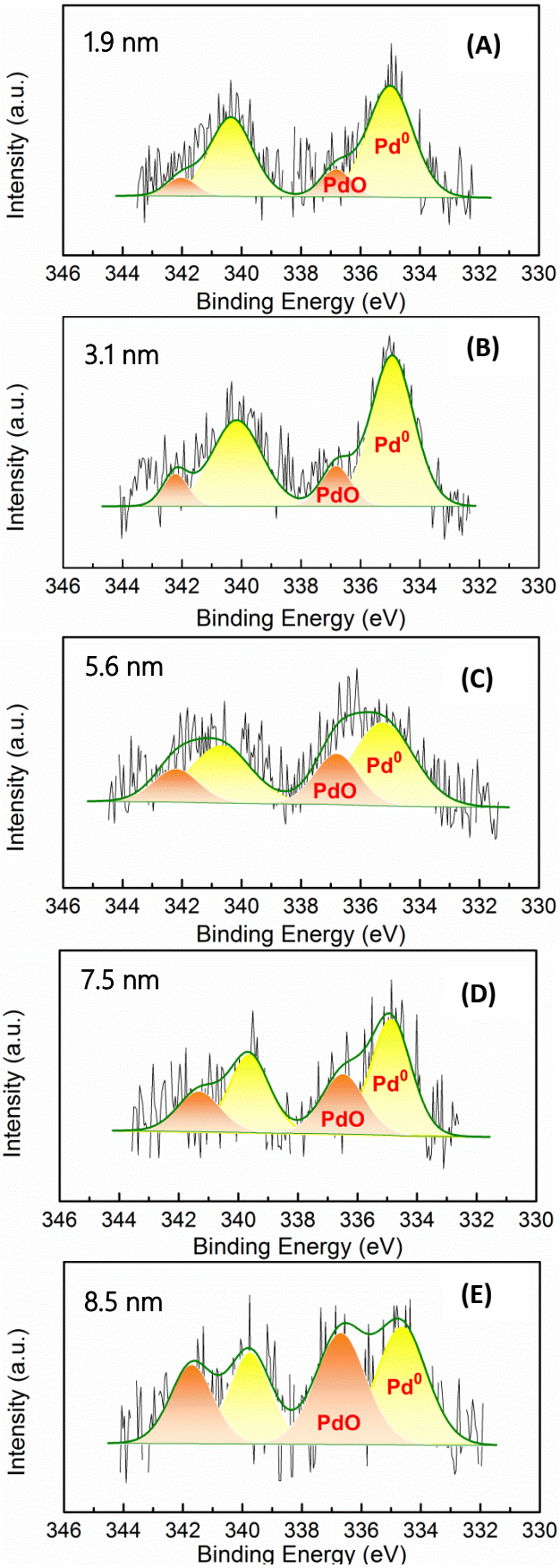

Fig. 7. Pd 3d photopeak recorded on Pd/Al-Ce(x) pre-activated at 500°C in the reaction mixture. (A) Pd/Al-Ce(550); (B) Pd/Al-Ce(800); (C) Pd/Al-Ce(850); (D) Pd/Al-Ce(900); (E) Pd/Al-Ce(950).

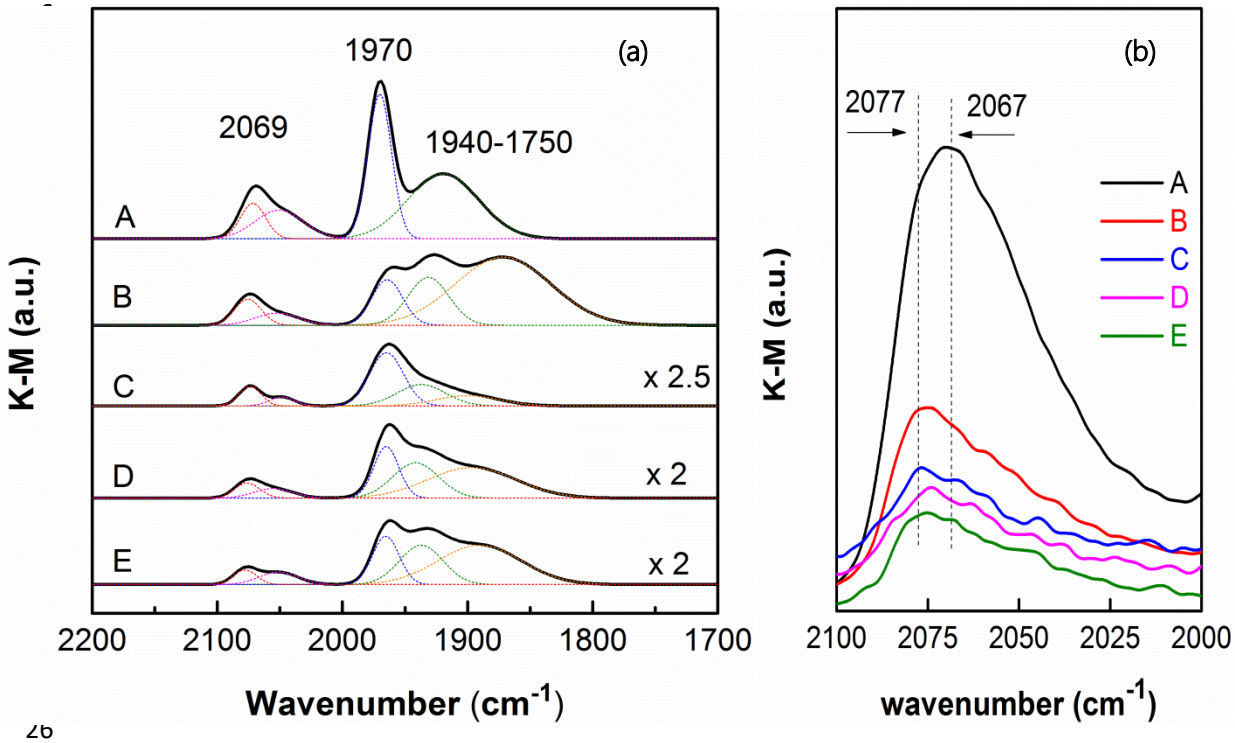

Fig. 8. (a) *In situ* FTIR CO adsorption on calcined Pd/Al-Ce(x). (b) IR range corresponding to linear-adsorbed CO on Pd atoms on corners with low coordination numbers or on Pd(111) facets. A: Pd/Al-Ce(550); B: Pd/Al-Ce(800); C: Pd/Al-Ce(850); D: Pd/Al-Ce(900) and E: Pd/Al-Ce(950).

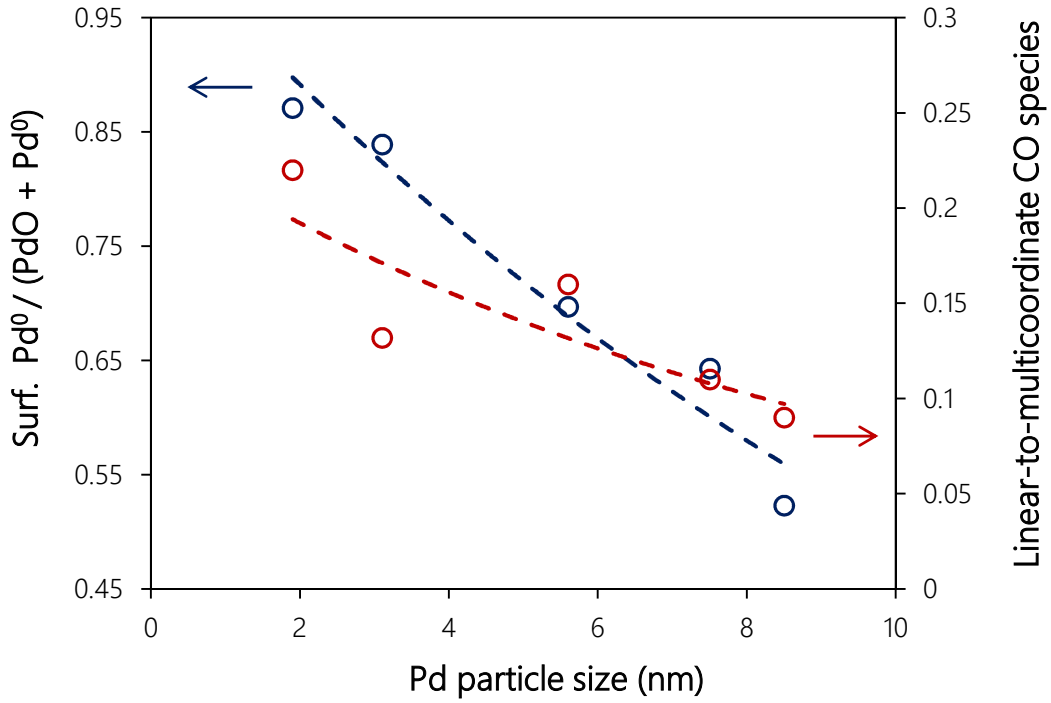

Fig. 9. Relationship between the metallic character of surface Pd species, particle size and morphology through the ratio between linear and multi-coordinated CO species.

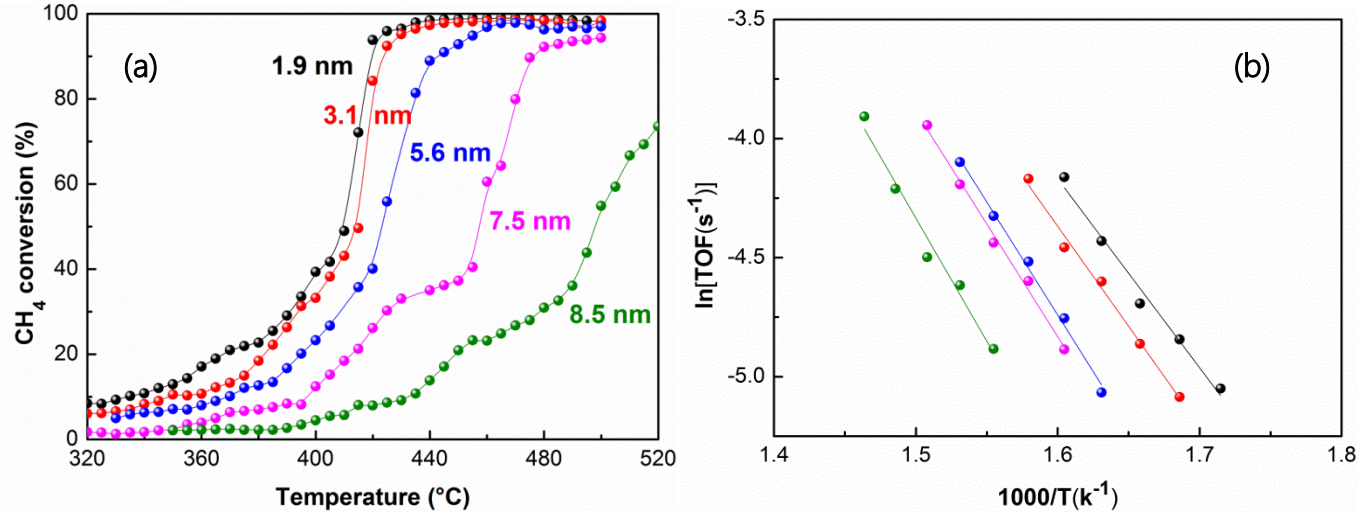

Fig. 10. (a) CH_4 light-off curves recorded on pre-activated monolithic Pd/Al-Ce(x) catalysts (50 g/ft^3). (b) Arrhenius plots for CH_4 conversion on pre-activated monolithic Pd/Al-Ce(x) catalyst (50 g/ft^3). Pd/Al-Ce(550) in black; Pd/Al-Ce(800) in red; Pd/Al-Ce(850) in blue; Pd/Al-Ce(900) in pink and Pd/Al-Ce(950) in green.

The samples were pre-activated under reaction gas at 500 °C for 5 h. Reaction conditions: 1000 ppm CH_4 + 5000 ppm CO + 930 ppm NO + 4035 ppm O_2 + 10vol. %CO_2 + 10vol. %H_2O balanced with N_2 (lambda=1); Gas hourly space velocity (GHSV) = 50,400 h^{-1} (~1680 mL min^{-1}).

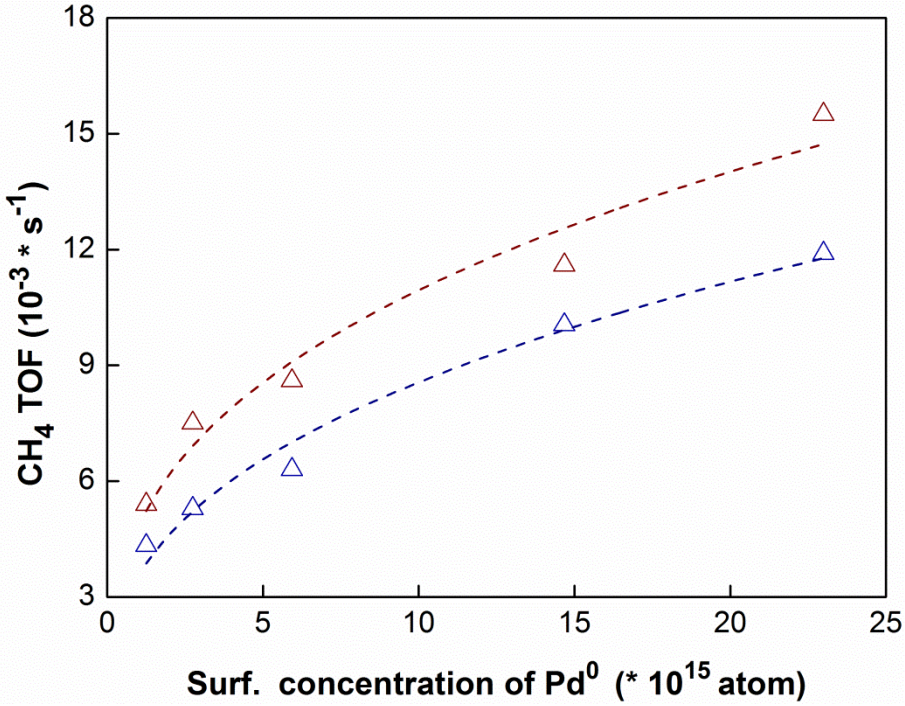

Fig. 11. The relationship between TOFs of CH_4 and the concentration of surface metallic Pd (TOF at 340 °C (Δ) and 350 °C (Δ))

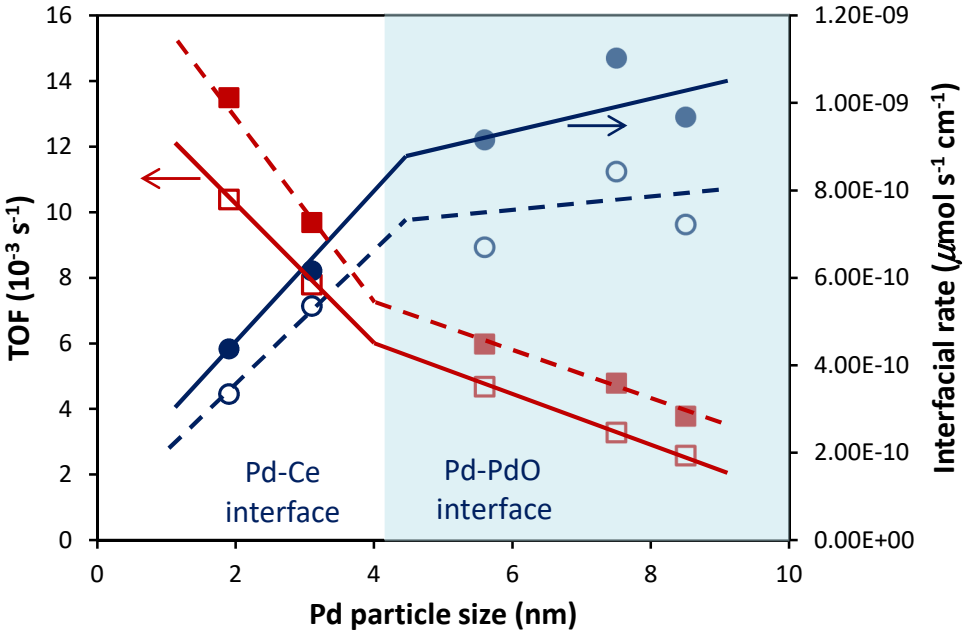

Fig. 12. Comparison of TOF and interfacial rates versus metallic Pd particle size: TOF (□) and interfacial rate (○) at 340 °C; TOF (■) and interfacial rate (●) at 350 °C.

Table 1. Physicochemical properties of calcined Pd/Al-Ce(x) catalysts.

Catalyst	BET surface area (m^2/g)	CeO_2 crystallite size [a] (nm)	PdO crystallite size [a] (nm)	Pd dispersion[c] D_{Pd} (%)	Pd particle size[d] d_{Pd} (nm)	Pd particle size[e] (nm)
Pd/Al-Ce(550)	132	5.3	n.d. [b]	40.7	2.7	1.9
Pd/Al-Ce(800)	126	6.7	n.d. [b]	28.9	3.8	3.1
Pd/Al-Ce(850)	126	8.9	7.3	17.7	6.2	5.6
Pd/Al-Ce(900)	119	9.2	9.0	14.9	7.4	7.5
Pd/Al-Ce(950)	115	8.6	10.9	11.9	9.2	8.5

[a] Obtained from XRD analysis
[b] Undetected from XRD analysis
[c] Calculated from CO chemisorption measurements assuming CO/Pd = 1
[d] Calculated from CO chemisorption measurements assuming spherical Pd particle
[e] From STEM measurements

Table 2. Oxygen uptake and released from TPO experiments on calcined Pd/Al-Ce(x).

Catalysts	O_2 released (heating) (μmol/g_{cat})	O_2 uptake (cooling) (μmol/g_{cat})
Pd/Al-Ce(550)	59.8	47.7
Pd/Al-Ce(800)	54.7	36.9
Pd/Al-Ce(850)	42.6	31.3
Pd/Al-Ce(900)	40	30.8
Pd/Al-Ce(950)	42.1	31

Table 3. Surface analysis from XPS on calcined and pre-activated Pd/Al-Ce(x) samples

Samples	Pd $3d_{5/2}$ B.E. (eV)		Relative Pd concentration (at.%)[a]		Surf. Pd^0/Pd^0+PdO (%)		Surf. $Ce^{3+}/Ce^{3+}+Ce^{4+}$ (%)	
	Calcined	Pre-activated	Calcined	Pre-activated	Calcined	Pre-ativated	Calcined	Pre-activated
Pd/Al-Ce(550)	336.7	336.8/335.2	0.49	0.44	~0	87.1	22.3	24.9
Pd/Al-Ce(800)	336.6	336.7/335.0	0.44	0.38	~0	83.9	21.7	23
Pd/Al-Ce(850)	336.5	336.7/335.1	0.29	0.24	~0	69.7	20.6	21.7
Pd/Al-Ce(900)	336.2	336.5/334.9	0.16	0.16	~0	64.3	17.2	18.1
Pd/Al-Ce(950)	336.0	336.4/334.9	0.09	0.13	~0	52.3	15.6	17.3

[a] Normalized by the sum of Pd, Ce, and Al

Table 4. Kinetic features of methane conversion on calcined Pd/Al-Ce(x) pre-activated under reaction mixture at 500°C.

Samples	Specific rate (10^{-6} mol g_{cat}^{-1} s^{-1})		$E_{apparent}$ (kJ mol^{-1})	TOF (10^{-3} s^{-1})		I_0 (cm g^{-1})[a]	Interfacial rate (μ mols^{-1}cm^{-1})	
	340°C	350°C		340°C	350°C		340°C	350°C
Pd/Al-Ce(550)	46.4	60.7	66.0	10.4	13.5	1.4×10^{13}	3.3×10^{-10}	4.4×10^{-10}
Pd/Al-Ce(800)	27.9	32.1	69.9	7.8	9.7	5.2×10^{12}	5.4×10^{-10}	6.2×10^{-10}
Pd/Al-Ce(850)	10.7	14.6	79.1	4.7	6.0	1.6×10^{12}	6.7×10^{-10}	9.2×10^{-10}
Pd/Al-Ce(900)	7.5	9.8	83.7	3.3	4.8	8.9×10^{11}	8.4×10^{-10}	11.0×10^{-10}
Pd/Al-Ce(950)	5	6.7	89.3	2.6	3.8	6.9×10^{11}	7.2×10^{-10}	9.7×10^{-10}

[a] Normalized Interfacial perimeter expressed per gram of Pd assuming a circular geometry at the interface

Graphical Abstract :